El Niño and Greenhouse Warming: Results from Ensemble Simulations with the NCAR CCSM

HEIN ZELLE *

KNMI, De Bilt, The Netherlands

DEOS, Delft, The Netherlands

GEERT JAN VAN OLDENBORGH
GERRIT BURGERS

KNMI, De Bilt, The Netherlands

HENK DIJKSTRA

Department of Atmospheric Science

Colorado State University, Fort Collins, USA

Submitted to Journal of Climate

February 17, 2005

*Corresponding author: Geert Jan van Oldenborgh, Department of Oceanographic Research, KNMI, P.O. Box 201, 3730 AE De Bilt, the Netherlands. Email: oldenborgh@knmi.nl

Abstract

The changes in model ENSO behavior due to an increase in greenhouse gases (according to the IPCC Business-As-Usual scenario) are investigated using a 62 member ensemble 140-year simulation (1940–2080) with the National Center for Atmospheric Research Community Climate System Model (CCSM, version 1.4). Although the global mean surface temperature increases by about 1.2 K over the period 2000–2080, there are no significant changes in the ENSO period, amplitude and spatial patterns. To explain this behavior, an analysis of the simulation results is combined with results from intermediate complexity coupled ocean-atmosphere models. It is shown that this version of the CCSM is incapable of simulating a correct meridional extension of the equatorial wind stress response to equatorial SST anomalies. The wind response pattern is too narrow and its strength is insensitive to background SST. This leads to a more stable Pacific climate system, a shorter ENSO period and a reduced sensitivity of ENSO to global warming.

1. Introduction

Interannual variations in the present climate strongly involve El Niño/Southern Oscillation (ENSO) in the Tropical Pacific. This phenomenon is caused by ocean-atmosphere interaction in the equatorial Pacific. The surface winds are influenced by the sea-surface temperature (SST) which subsequently affect the ocean currents and ocean heat transport causing changes in SST. The time scale of variability is determined by ocean adjustment processes (Philander, 1990; Neelin et al., 1998; Dijkstra and Burgers, 2002).

From proxy data, more and more information becomes available on the behavior of ENSO under different global mean temperatures. Based on the analysis of annually banded corals from Papua New Guinea, Tudhope et al. (2001) show that ENSO has existed for the past 130ka. However, there have been substantial changes in its strength through time. Based on analysis of Ecuadorian varved lake sediments, Rodbell et al. (1999) find that ENSO periods were larger than 15 year during the interval 15ka - 7ka and that modern periodicities of 2 - 8 years appeared afterwards. Data from microfossils show that ENSO events were less intense around 3ka but more pronounced around 1.5 ka (Woodroffe et al., 2003).

The variations in strength of ENSO events over the last 150 years are better known from observational data. According to NCEP data, the standard deviations of the Southern Oscillation Index (SOI, normalized sea level pressure difference between Darwin and Tahiti) and the NINO3.4-index (SST anomalies averaged over the region 5°S–5°N, 170°W–120°W) for 1951–1975 were 1.59 ± 0.14 and 0.78 ± 0.07 respectively, and 1.82 ± 0.19 and 0.95 ± 0.09 for the period 1976–2000. The error margins indicate the 95% confidence level interval. This shows that the amplitude of these indices has increased (for NINO3.4 this is partly due to better sampling since 1980), raising concern that ENSO may be intensifying as a result of global climate change (Trenberth et al., 1997).

Model studies of the behavior of ENSO in a warmer climate show conflicting results. In some early studies using coarse resolution models (Knutson et al., 1997), the mean zonal sea-surface temperature gradient decreased with little change in El Niño-like activity. In other early models (Timmermann et al., 1999), increasing greenhouse gas concentrations induced a more El Niño like mean state with more pronounced cold events than warm events. In the second version of the Hadley Centre model (HadCM2), changes in El Niño activity, frequency and phase locking are found. However, in the new version of the Hadley Centre model (HadCM3), no changes in El Niño statistics are found (Collins, 2000). This is attributed to the differences in physical parameterization and not to the differences in resolution between the two versions of the model. In one coupled model (Noda et al., 1999), a change towards a more La Niña state is found. The credibility of the predictions of the response to global warming in the coupled models (an overview of the models is given in Latif et al., 2001) is also undermined by the lack of confidence in their simulation of cloud feedbacks.

One of the most comprehensive models used for studying the behavior of ENSO under different global mean temperatures is the NCAR - CCSM (Otto-Bliesner and Brady, 2001; Huber and Caballero, 2003). The model ENSO variability under present climate conditions was studied in Otto-Bliesner and Brady (2001) using a 300 year simulation. The warm-pool/cold-tongue equatorial temperature gradient has a realistic amplitude. However, the cold tongue is located too far to the west and the mean SST is too symmetrical with respect to the equator. The equatorial thermocline is slightly more diffusive than in observations. There is a reasonable simulation of the amplitude, phase and propagation features of the SST anomalies and thermocline anomalies. SST anomalies appear as a standing pattern whereas there is a slight eastward propagation of anomalies at the depth of the thermocline. The variability in the model is largest in the NINO3.4 region with a standard deviation of 0.77 K. The wavelet power spectrum shows that the period is in the 2–4 year range and hence relatively short compared with observations, which show a more diffuse spectrum with a period between 3–8 years.

There have been two modelling studies of the Last Glacial Maximum with this model. Otto-Bliesner et al. (2003) report 2.1 K cooling in the tropical Pacific Ocean compared to present-day conditions, a reduced east-west gradient and a sharper thermocline; ENSO activity is enhanced by 20%. Recently, Peltier and Solheim (2004) in a much longer experiment found equatorial SST about 4.5 K below present-day values. They find very little changes in ENSO characteristics. The only change is that the amplitude of SST variability increases by 25% in the Niño3 region.

In this study, we address the question of changes in ENSO behavior under an increasing global mean temperature. We use results from a 62 ensemble member simulation of the CCSM version 1.4 over the period 1940–2080, using the IPCC Business-As-Usual scenario for greenhouse gas forcing after 2000. The choice for this model version was motivated by computational constraints, the fact that it was carefully tuned to simulate the ENSO phenomenon rather well (Otto-Bliesner and Brady, 2001) and the relatively small effort involved in preparing the model system for our purpose. The procedure of the ensemble simulations is outlined in section 2, the results on the tropical Pacific climate system and its variability are presented in section 3. In section 4, we perform a detailed analysis using results from intermediate coupled ocean-atmosphere models which leads to the interpretation of the results from section 3. A summary and discussion is provided in section 5.

2. Global warming in the ensemble simulations

a. Model

The CCSM version 1.4 is a global climate model containing a primitive equation ocean and atmosphere model, a sea-ice model and a land-surface model. We have used the configuration as in Ammann et al. (2005). The atmosphere was run at T31 resolution (equivalent to a grid spacing of $3.75° \times 3.75°$) in latitude and longitude with 18 levels in the vertical and the highest model level at about 35 km. The land surface model distinguishes between specified vegetation types and contains a comprehensive treatment of surface processes. The ocean model was run using a grid with 25 vertical levels and a longitudinal resolution of 3.6°. The latitudinal resolution changes from 0.9° in the tropics to 1.8° in higher latitudes. The near equatorial meridional resolution is slightly coarser than that used in the ECHAM4/OPYC simulation (0.5°) by Timmermann et al. (1999). The sea-ice model includes sea-ice thermodynamics and sea-ice dynamics. The coupled system does not require artificial corrections in the heat exchange between atmosphere and ocean to simulate a reasonable climate state wih surface temperature bias below 2 K in most of the oceans (Boville et al., 2001).

An initial state (at 01-01-1940) was obtained from the simulations of Ammann et al. (2005). The coupled simulation was started under 1870 atmospheric composition conditions and integrated for 100 years. The atmospheric composition was then prescribed for the 1870-1940 period. This resulted in the initial state used as the starting point for the ensemble simulations. The climate system was integrated 62 times over the period 1940–2080. During the historical part of the simulation (1940–2000), greenhouse gas (GHG) concentrations, sulphate aerosols, solar radiation and vulcanic aerosols were prescribed according to observational estimates, kindly provided by C. Ammann (Ammann et al., 2005). From 2000 onwards, the solar constant and sulphate aerosols were kept fixed. Only the GHG concentrations varied according to the IPCC Business-As-Usual scenario which is similar to the SRES-A1 scenario (Dai et al., 2001). The ensemble members differ only in a small random perturbation in the initial temperature field of the atmosphere, enough to lead to entirely different atmospheric evolutions within the first couple of weeks of the integrations. In the following analysis, the first 10 years (1940–1949) of the simulation have been discarded to remove any remaining model spinup effects.

b. Changes in the global mean state

Fig. 1 shows the global mean surface air temperature as simulated by all 62 members, the ensemble mean and an observational estimate obtained from the Climatic Research Unit (CRU, Jones et al., 2001). The simulated temperatures cover the observations very well. The effects of the volcano eruptions of the Agung (1963), El Chichon (1982) and Pinatubo (1991) are clearly visible as a temporary cooling on the order of several tenths of a degree. The temperature rise after 2000 is solely due to the increasing concentrations of GHGs. Between 2000 and 2080 the global mean temperature has risen 1.2 K, extrapolating the rise from 1990 to 2100 leads to a global warming of about 1.7 K.

The difference pattern of the ensemble mean temperature averaged over the 30-year periods 2050–2080 and 1950–1980 is plotted in Fig. 2a. Warming of up to 5 K occurs in the region north of 40°N. In the equatorial Pacific the warming is less strong at about 1 K, the western equatorial Pacific heats up 0.2 K more than the eastern equatorial Pacific. The changes in precipitation between the 1950–1980 and 2050–2080 periods are shown in Fig. 2b as a percentage of the 1950–1980 mean. The largest relative changes are found over the Sahel, Antarctica, Greenland, the northern Indian ocean and the equatorial Pacific. In the western equatorial Pacific precipitation increases by about 2mm/month.

Compared to other models that have been used in the IPCC Third Assessment Report (IPCC, 2001, Chapter 8: Model Evaluation), the CCSM configuration used here is on the low end with respect to sensitivity to GHG forcing. The extrapolated 1.7 K global temperature increase between 1990–2100 is just above the lower bound established in the TAR (1.4 K to 5.8 K) based on results from different model simulations and emission scenarios. The patterns of change in temperature and precipitation (up to 2080) have comparable features with those of the other models.

3. ENSO and Global Change

From the total data set emerging from the ensemble simulations the equatorial Pacific region was extracted, in particular for the variables zonal wind stress τ^x, the depth of the 20°C isotherm Z_{20} and the sea-surface temperature SST. The domain used is 12°S–12°N, 120°E–80°W. Because the time mean state of the equatorial Pacific, the seasonal cycle and ENSO variability are strongly linked, we present the changes in each of them subsequently in the following paragraphs.

The ensemble mean sea-surface temperature averaged over the period 1950–1980 is shown in Fig. 3b, to be compared with ERA-40 reanalysis data (Uppala and coauthors, 2005) in Fig. 3a. Although the overall features of the cold tongue/warm pool agree reasonably well with observations, there are several deficiencies similar to those in the single simulation described by Otto-Bliesner and Brady (2001). The cold tongue extends too far to the west and the SST pattern is too symmetrical about the equator: there is little SST variability south of the equator near the South-American coast. The differences in SST between the periods 2050–2080 and 1950–1980 are shown in Fig. 3d. There is a nearly homogeneous warming of the tropical Pacific with a slight increase in the equatorial east-west temperature gradient as the western part warms about 0.2 K more than the eastern part.

The ensemble mean seasonal cycle of SST for the period 1950–1980 is shown in Fig. 4b, the same for ERA-40 reanalysis data in Fig. 4a. The semi-annual signal in the western Pacific and the annual signal in the eastern Pacific are simulated reasonably well. The timing of the maximum SST in spring is a bit too late but the westward propagation of SST anomalies is

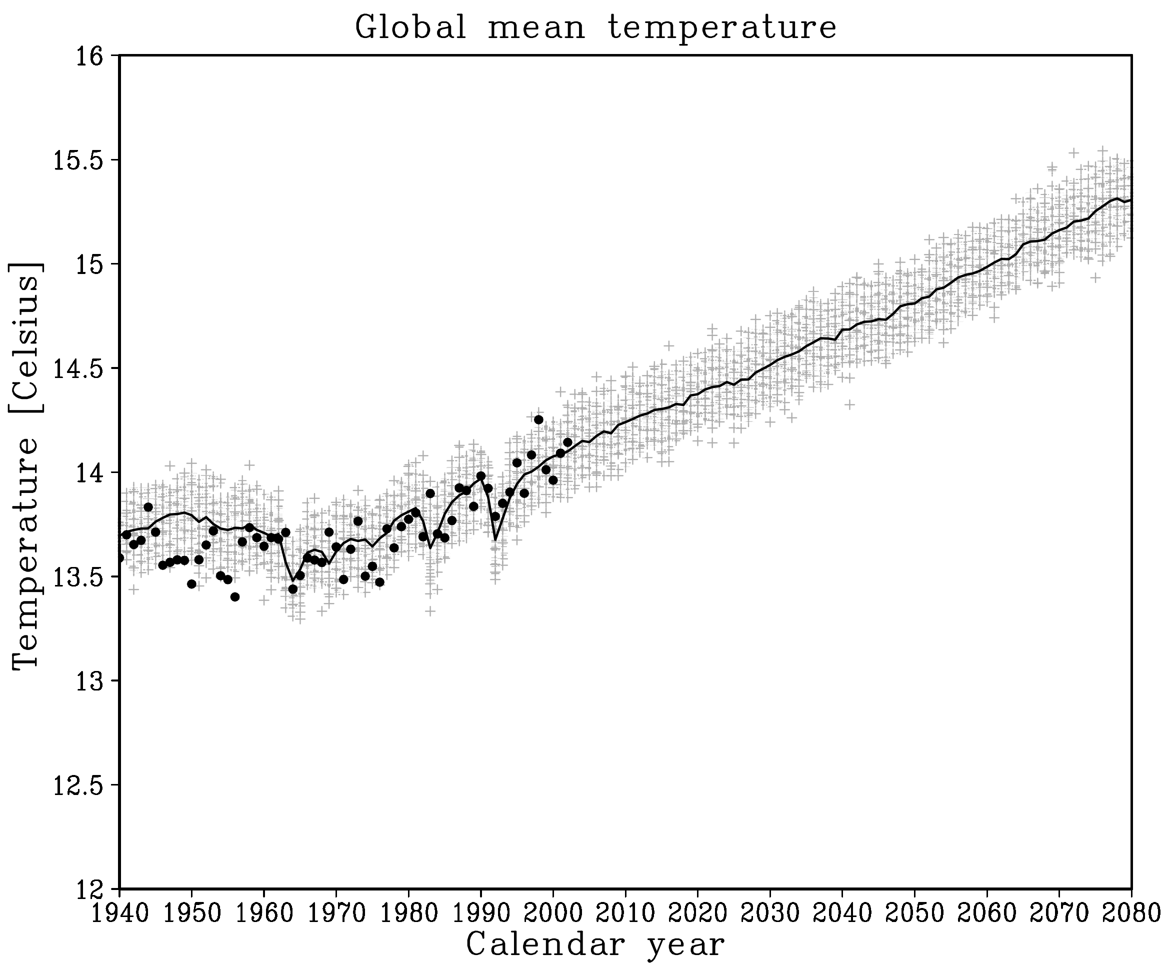

Figure 1: Global mean temperatures of all 62 simulations (light crosses), the ensemble mean (solid line) and observed temperatures from the Climate Research Unit (dark dots). The CRU timeseries obtained are anomalies with respect to the 1960–1990 period. We added the ensemble mean simulated temperature over this period.

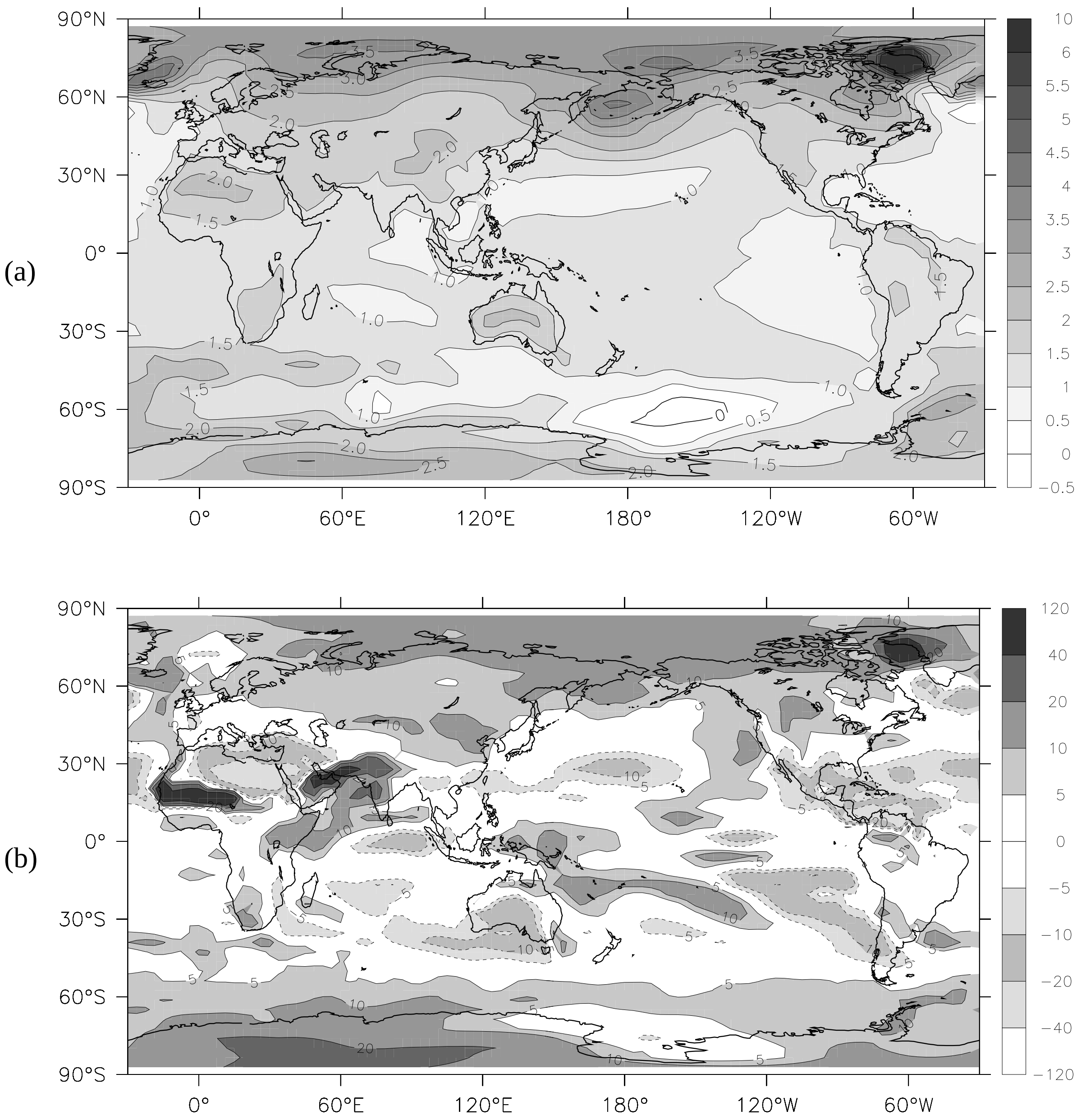

Figure 2: Difference of (a) ensemble mean surface temperature (K) and (b) ensemble mean precipitation (%) between the 30-year periods 2050–2080 and 1950–1980.

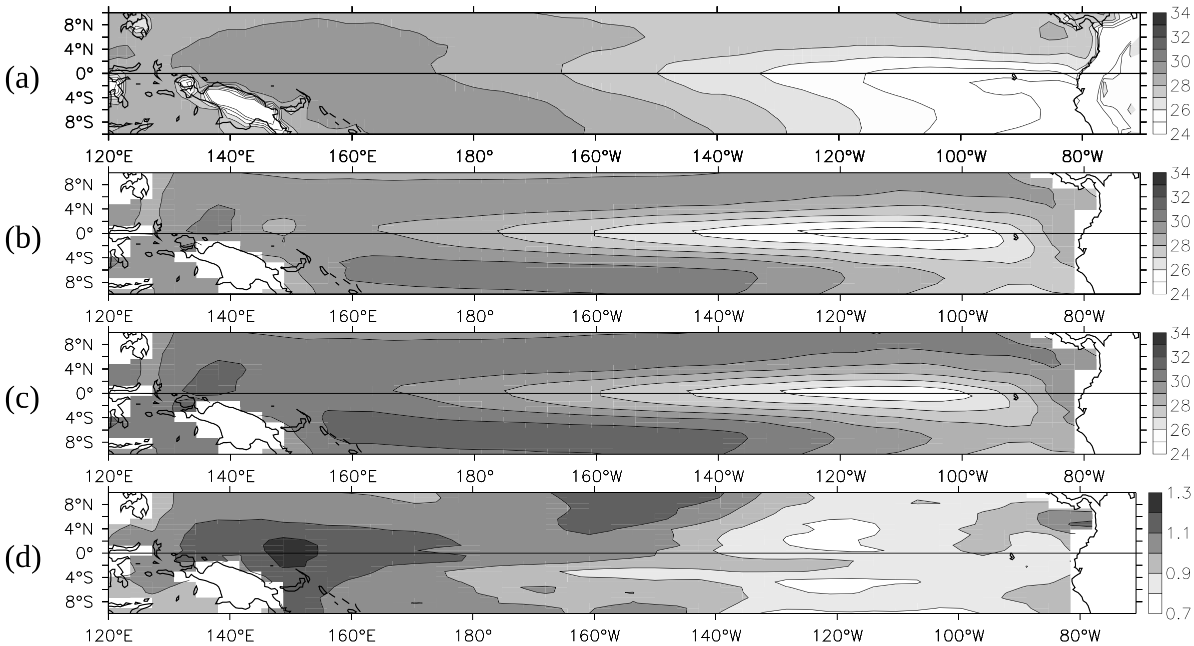

Figure 3: (a) Annual mean sea surface temperature in the equatorial Pacific from ERA-40 reanalysis data. (b) CCSM simulations, 1950–1980 ensemble mean, (c) the same for the period 2050–2080 and (d) difference of (c) and (b).

in accordance with observations. The differences in the seasonal cycle of SST between the periods 2050–2080 and 1950–1980 are shown in Fig. 4d. The figure confirms that the western Pacific is warming up more than the eastern Pacific, otherwise the warming is almost homogeneous. We do not find an intensification of the seasonal cycle as discussed by Timmermann et al. (2004).

A similar analysis of thermocline depth shows no significant differences between the periods 1950–1980 and 2050–2080. There is a slight deepening of the equatorial thermocline of approximately 6 m in the western Pacific and approximately 3 m in the eastern Pacific. Changes in surface wind stress are also negligible.

As already mentioned in Otto-Bliesner and Brady (2001), the variability of the ENSO indices is slightly smaller than what is observed. For the first ensemble member, SST averaged over the NINO3.4 region is shown in Fig. 5a together with an estimate of the trend of the ensemble. The detrended NINO3.4 SSTA index with seasonal cycle removed is shown in Fig. 5b. The amplitude is simulated reasonably well with a standard deviation of 0.77 ± 0.01 K for the period 1970–2000, but there is more high frequency noise and the oscillation is more regular than the observed NINO3.4 index. The standard deviation was computed for the whole ensemble, but individual members show very similar results. The skewness of the detrended NINO3.4 index for the period 1970–2000 is -0.05 ± 0.02 compared to 0.40 ± 0.25 for the NCEP NINO3.4 index: ENSO is almost symmetrical in the CCSM. The amplitude of thermocline variability in the NINO3.4 region for the period 1970–2000 is too small: 5.6

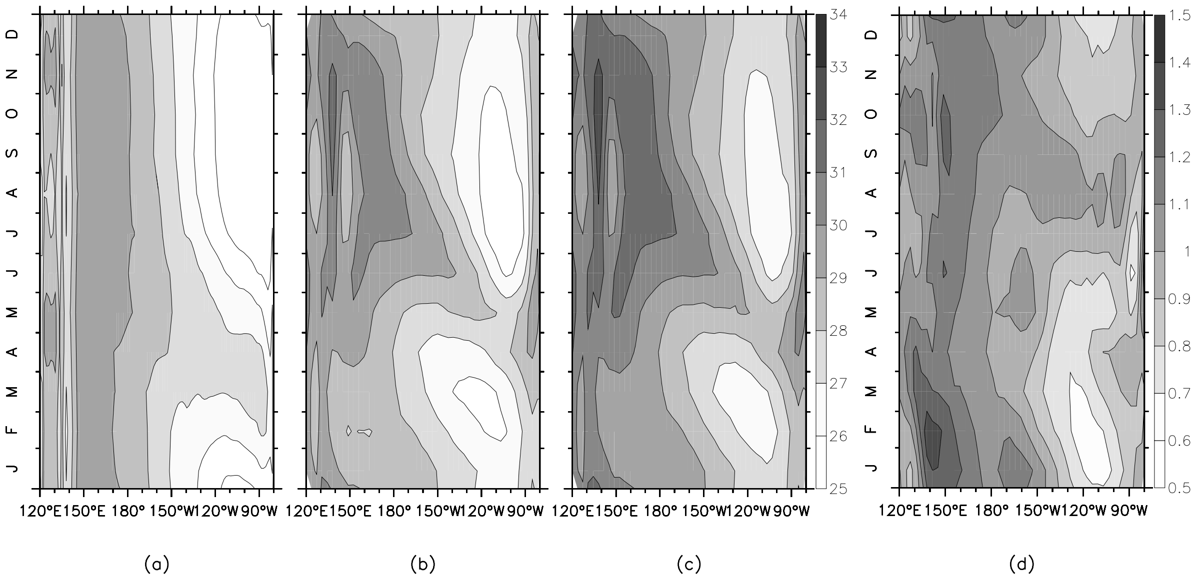

Figure 4: (a) Seasonal cycle of the sea-surface temperature in the equatorial Pacific from ERA-40 reanalysis data. (b) CCSM simulations, 1950–1980 ensemble mean, (c) the same for the period 2050–2080 and (d) the difference of (c) and (b).

m compared to 13.0 ± 1.5 m from TAO/TRITON observations (McPhaden et al., 1998). The amplitude of τ^x variability in the NINO4 region (160°E–150°W, 5°S–5°N) is also weaker than observed: $6.5\;10^{-3}$ Pa compared to $(14 \pm 1)\;10^{-3}$ Pa in the TAO/TRITON observations.

A wavelet spectrum (based on a Morlet-6 transform) indicates that most of the energy is contained in the frequency band of 2.5–3.5 year. Weaker energy in this band occurs during the early and mid 1990's and between 2050 and 2060 (Fig. 6a). Spectra based on two thirty-year intervals, averaged over all ensemble members, indicate that the period of ENSO variability is around 2.8 year (Fig. 6b) for both intervals. In each spectrum of the individual members, there appears to be no significant change in ENSO period and amplitude. Together with the results in Fig. 5, this strongly suggests that ENSO variability in this version of CCSM does not change under a moderate global warming.

The pattern of variability associated with ENSO can be determined through the first EOF of SST and is plotted in Fig. 7b for the 1950–1980 period. It broadly resembles the observed variability (Fig. 7a), again with deficiencies in the cold tongue region and the equatorial asymmetry like in Fig. 3. The first EOF explains 41% of variance, against over 60% in the observations. Neither this EOF pattern nor the second one (not shown) changes over the period 2050–2080 (Fig. 7c), confirming once more that the ENSO variability is only marginally affected by the global temperature increase.

A simple conclusion from these results would be that ENSO does not change in a warmer climate. This is in agreement with most studies in state-of-the-art climate models (Collins and coauthors, 2005), such as those used in the IPCC TAR and summarized in Latif et al.

(a)

(b)

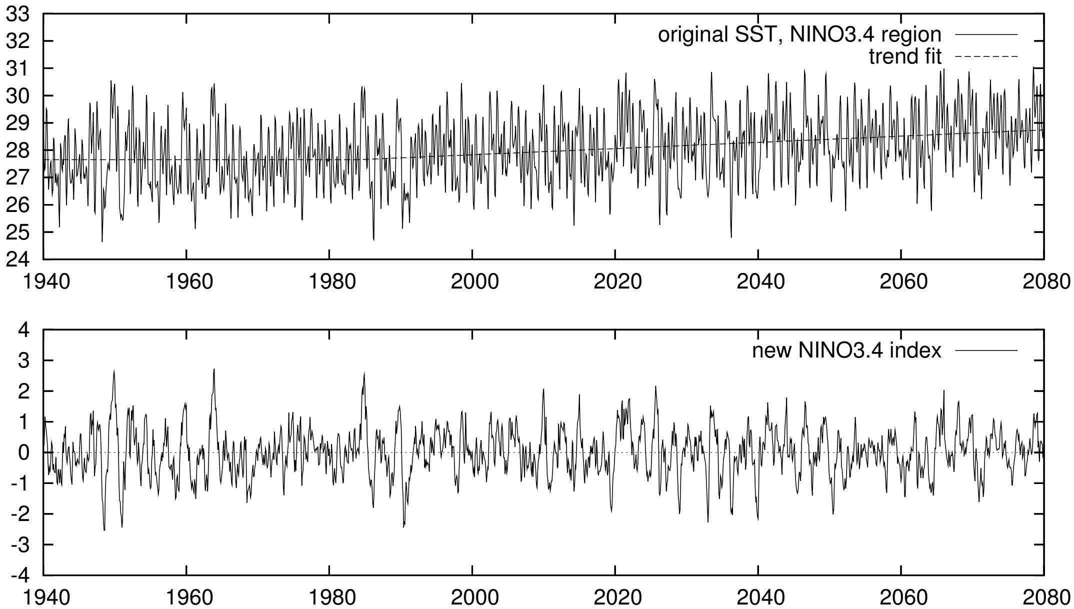

Figure 5: (a) SST values in the NINO3.4 region for ensemble member 1 of the CCSM, with an estimate of the ensemble trend. (b) The detrended NINO3.4 SSTA index for ensemble member 1, with seasonal cycle removed.

(2001). However, there are a few suspicious features which motivate further analysis into the reasons why ENSO does not change in the CCSM simulations. Although the mean state cold-tongue/warm-pool configuration is reasonably simulated, the ENSO period in the CCSM is smaller than that observed. Furthermore, ENSO under greenhouse warming conditions appears to be more regular than what is observed, suggesting that the strength of the coupled feedbacks as found in intermediate complexity coupled models (ICMs) is weaker in the CCSM results. Finally, as will be shown below, the equatorial wind response to SST has some deficiencies with respect to observations. In the next section, we will analyze and interpret the CCSM results through a comparison with results from ICMs.

4. Analysis

In this section, our main point is to demonstrate that the insensitivity of ENSO to global warming in the CCSM is due to deficiencies in the simulation of the equatorial zonal wind stress response. First we will show that the ENSO behavior in the CCSM is likely to be that of a noise-driven stable system. Next, ICMs are used to demonstrate that an enhanced stability of the Pacific climate state and a shorter ENSO period can both be explained by a zonal wind stress field that is strongly confined in the meridional direction. An analysis of the CCSM results will show that the wind stress field is indeed too narrow around the equator, and that the wind response is independent of background SST.

(a)

(b)

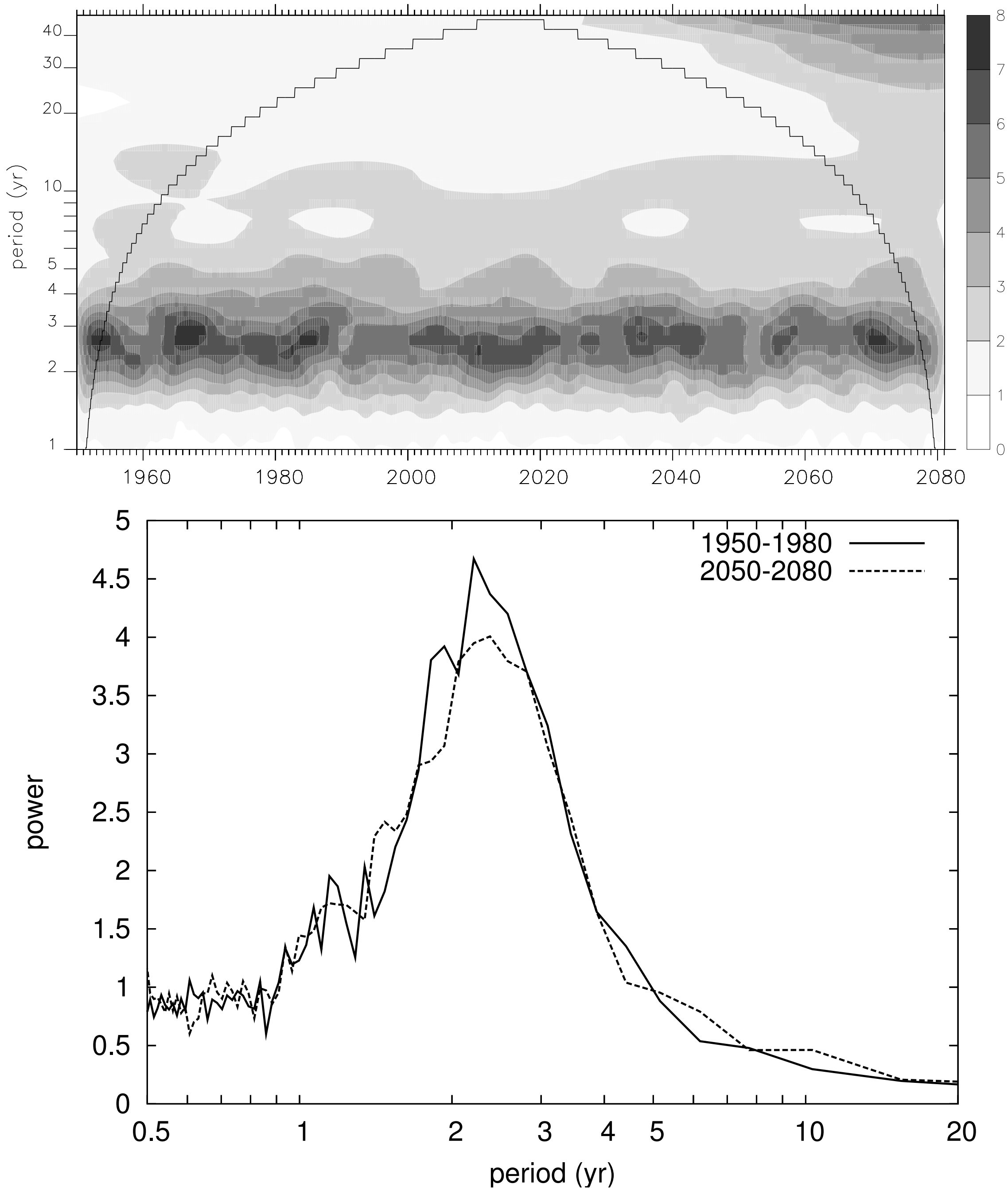

Figure 6: (a) Wavelet spectrum (Morlet-6) of the NINO3.4 index of the ensemble simulations. (b) Spectra of the NINO3.4 index for two thirty-year periods, averaged over all ensemble members.

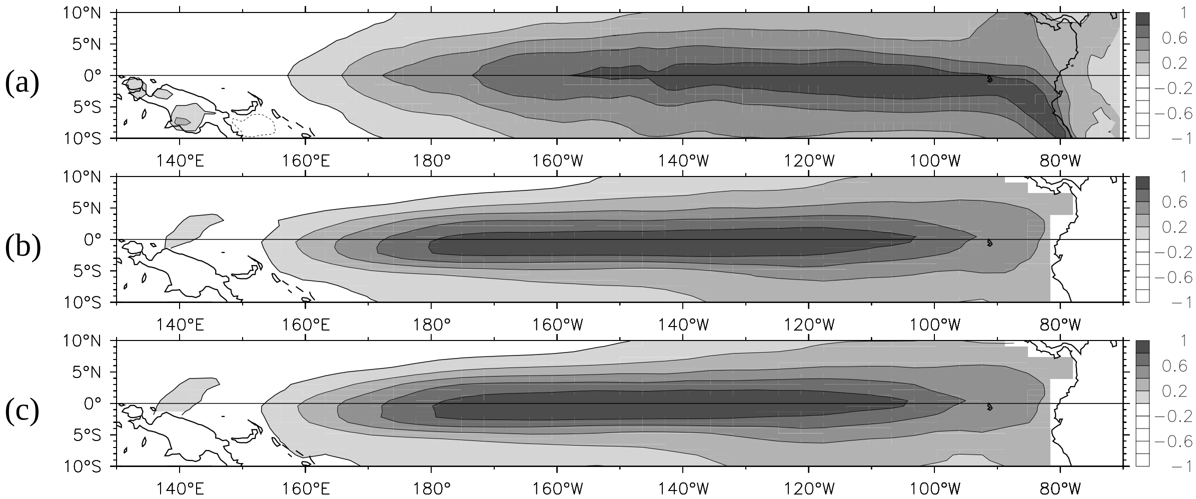

Figure 7: (a) First EOF of SST in the equatorial Pacific from ERA-40 reanalys data. (b) CCSM simulations, ensemble mean over the period 1950–1980 and (c) for the period 2050–2080.

a. Low-order chaos versus noise driven

In the theoretical framework that has been developed to describe ENSO variability, a Hopf bifurcation marking the transition from a stable stationary time-mean state to a periodically varying state is of central importance (Neelin et al., 1998). The transition from stable to unstable can, for example, be induced by varying the strength of coupled feedbacks in the equatorial Pacific, such as the amplitude of the wind anomaly per degree SST anomaly. The spatial and temporal pattern of the periodically varying state of ENSO can be estimated from observations, even if there are substantial secondary modes (Jiang et al., 1995).

Estimates from observations indicate that ENSO is close to neutral in reality (Fedorov and Philander, 2000; Dijkstra and Burgers, 2002) and, in addition, is quite irregular; this leaves two possibilities. The first possibility is that the Pacific climate state is linearly unstable, that the ENSO amplitude is determined by non-linear dynamics, and that deterministic chaotic dynamics cause its irregularity. In this case, ENSO is qualitatively a low-order chaotic system. The second possibility is that at the root of ENSO lies a linearly stable Pacific climate system, with atmospheric noise exciting finite-amplitude fluctuations inducing the irregularity of ENSO. In this case, ENSO is qualitatively a noise-driven stable system. Philander and Fedorov (2003) argue that the latter is most likely what occurs in nature. The term ‘noise’ refers to processes that have much smaller spatial and time scales than ENSO and evolve independently. The complete system (deterministic + noise) has many degrees of freedom.

We have investigated whether ENSO in the CCSM is a low-order chaotic system or not with the method of Tziperman et al. (1994), described in the Appendix. They showed, for example, that the Zebiak-Cane model (Zebiak and Cane, 1987) with standard parameter settings is a low-order chaotic system. The method estimates the dimension of the attractor from time series of a characteristic variable. The dimension is obtained from the slope of the cumulative

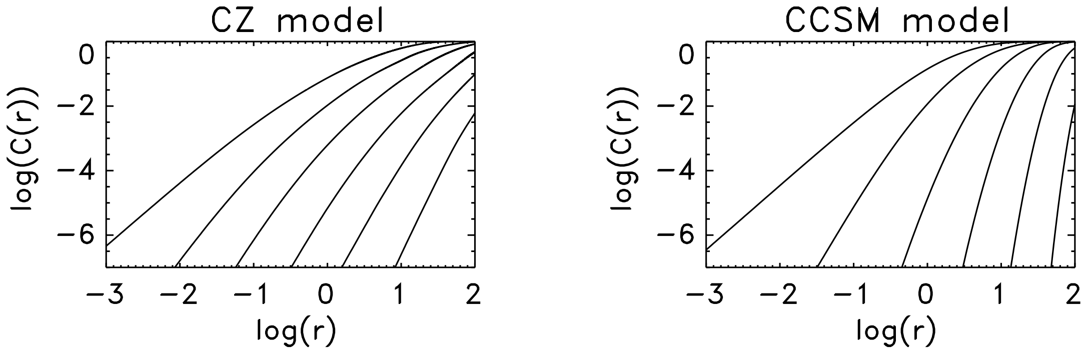

(a) (b)

Figure 8: Estimates for the dimension of the attractor of a run of the Zebiak-Cane model (a) and the CCSM ensemble simulations (b). From left to right, curves are shown for embedding dimensions M of 2, 4, 8, 16, 32 and 64. The estimate equals the value of the slope of the straight section of the curves in the limit of high embedding dimension and run length. Because the run length is limited (8742 years for both Zebiak-Cane and CCSM), no meaningful estimates can be made beyond an embedding dimension of around 30.

distribution function $C_2(r)$ versus the distance between points r in a log-log plot. When the slopes for increasing embedding dimension M converge to a finite value, the attractor dimension is finite and a low-order chaotic system is causing the behavior (see the Appendix for details).

We compared the results for the period 1950-2080 of the CCSM ensemble, 8742 simulated years in total, with a simulation of the Zebiak-Cane model of the same length. As characteristic model variables we took values of the NINO3 index in the Zebiak-Cane model run and of the NINO3.4 index in the CCSM ensemble members, averaged over 3 month intervals. For the Zebiak-Cane model we see that the slopes in Fig. 8a slowly converge to an attractor dimension of around 5. This is in agreement with Tziperman et al. (1994) who obtained an estimate of 3.5 from embedding dimensions up to 14. For the CCSM simulations (Fig. 8b) there is no sign that the slopes converge and we can only establish a lower bound of about 40 for the attractor dimension.

We conclude that the NINO3.4 behavior in the CCSM simulations is qualitatively similar to that of a stable noise driven system, and does not show dynamics characteristic of a low-dimensional chaotic system.

b. Sensitivities in ICMs

To find the reason for the stability of the Pacific climatology on the one hand and the relatively small ENSO period on the other hand, sensitivity studies which have been done with ICMs are useful. One of the ICMs that has been used to study the stability of the Pacific climate system is the IPSM model of Van der Vaart et al. (2000). The IPSM is a pseudo-spectral model very similar to the Zebiak and Cane (1987) model in that it couples an ocean model consisting of a shallow-water layer with an embedded mixed layer of fixed depth to a Gill (1980) atmosphere model.

Both the mean climate and the stability properties of this state change when parameters like the strength of the coupling feedbacks, say μ, are varied. Such parameters are therefore ideally suited for studying sensitivities of ENSO behavior to certain physical processes. For small μ, the steady climate states are stable but above critical values of μ, spontaneous oscillatory behavior appears through the destabilization of Pacific climatology to the ENSO mode. This transition can be shown to be a Hopf bifurcation and in Van der Vaart et al. (2000), the position of the Hopf bifurcation and the period of the ENSO mode at criticality was determined over a broad range of parameter space.

One of the interesting results in Van der Vaart et al. (2000) is replotted in Fig. 9. Here, the value of μ at the Hopf bifurcation, μ_c, as well as the period of the ENSO mode at criticality, P_c, are plotted versus the ratio of the oceanic and atmospheric Rossby deformation radii, α. Cane et al. (1990) perform a similar analysis for a more idealized model. As α increases, the meridional extent of the atmospheric wind-stress response decreases and becomes more localized near the equator. From Fig. 9a we see that with increasing α, the cold tongue/warm pool mean state stabilizes as the Hopf bifurcation shifts to larger values of μ. At the same time the period at criticality decreases, because the forced Rossby waves participating in the adjustment of the ocean do not include the high wavenumber slow modes further away from the equator (Kirtman, 1997). Guilyardi et al. (2004) find that also in coupled GCMs the width of the wind response determines the ENSO period. A higher resolution atmosphere GCM increases the meridional extent of the wind response pattern and leads to a more realistic ENSO simulation.

Although only the dependence of the critical conditions on the meridional extent of the wind stress is considered, the results in Fig. 9 strongly motivate us to look further into the effects of the meridional pattern of zonal wind on the ENSO period and the stability of the Pacific climate state. To investigate this in more detail, we make use of a linear shallow-water ocean model, the Gmodel as presented in Burgers et al. (2002), coupled to a Gill atmosphere model (Gill, 1980).

In the Gmodel, the reduced-gravity ocean model is forced by zonal and meridional wind stress, and has thermocline depth, zonal and meridional current as output variables; SST is computed only as a diagnostic variable. The Gmodel has been tuned to simulate the observed NINO3 and NINO4 indices well when forced with FSU pseudo wind stress fields (Stricherz et al., 1997). We have also fitted the parameters of the SST equation to the CCSM ocean model; these parmeters give essentially the same results. The atmosphere model responds only to the simulated SST field. The response to an SST spike (very narrow in the zonal direction) on the equator is computed with the Gill model (Gill, 1980). The full wind response is obtained by integrating along the equator and multiplying the local SST anomaly with this wind response pattern. The meridional scale of the wind response to SST anomalies can be adjusted with the parameter α, the ratio of the oceanic and atmospheric Rossby deformation

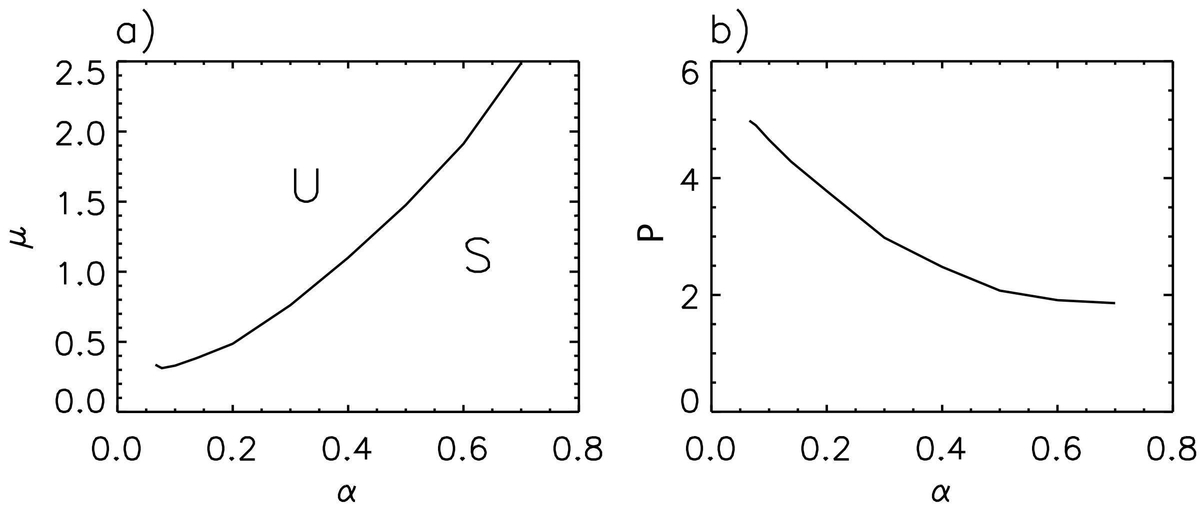

Figure 9: (a) The value of the critical ocean-atmosphere coupling strength μ_c at the Hopf-bifurcation as a function of α, the ratio between the oceanic and atmospheric Rossby radii. S (U) indicates regions of linear (un)stable climatologies. (b) The period P of the oscillation (in years) at the Hopf-bifurcation as a function of α.

radii.

To determine the relation between the ENSO period and the meridional extent of the zonal wind response, three Gmodel runs were performed with different values of α. For each run, the coupling strength μ was set just below the critical value μ_c. A Hovmüller diagram of SST is plotted for different values of α in Fig. 10. It is clear that the ENSO period decreases with increasing α (decreasing meridional extent): the period goes down from approximately 8 years to 21 months. The critical coupling strength μ_{C} increases with increasing α, consistent with the results in Fig. 9a.

c. The wind response in the CCSM

Given that the Pacific climate state in the CCSM appears very stable and the ENSO period is shorter than that observed, the results in the previous section motivate us to investigate the wind response to SST anomalies in the CCSM and to compare this response with observations and with results from the Gmodel.

The response of zonal wind to SST anomalies has been found by a straightforward linear regression (see for example the textbook of Von Storch and Zwiers (1999,2001), §8.3) on the monthly data: $\tau_x'(\mathbf{x}) = \int d\mathbf{x}'\ A(\mathbf{x},\mathbf{x}')\ T'(\mathbf{x}')$. Here τ_x' and T' are the surface fields of zonal wind stress anomalies and SST anomalies in the equatorial Pacific region, and the function A is the response model. Because the model is underdetermined even for the large ensemble considered, the dimension has to be reduced. This was achieved by averaging T' over boxes on the equator. The large amount of data from the CCSM simulations ($\sim 10^5$ months) allows up to eight boxes along the equator, but for a comparison with observational data we use only

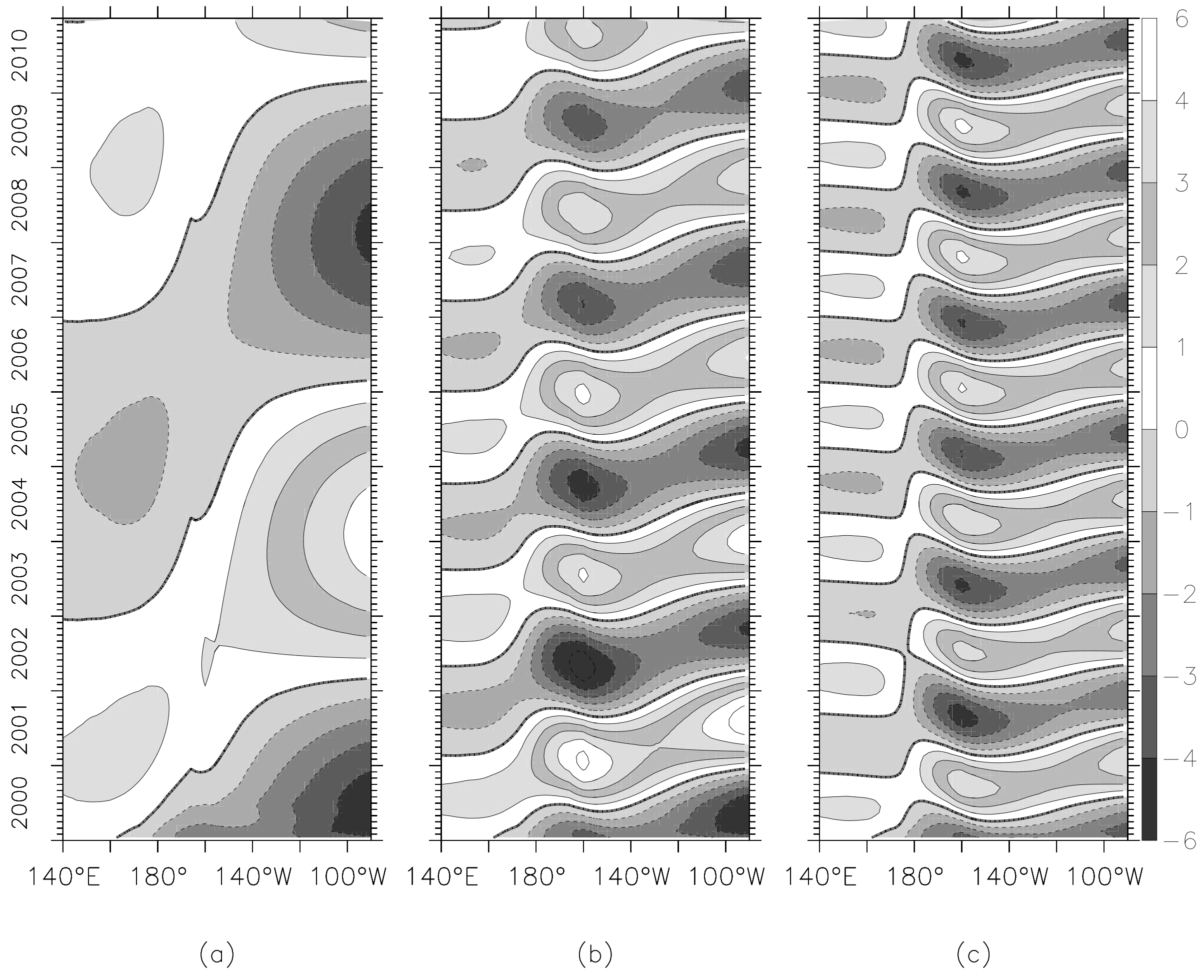

Figure 10: Hovmüller diagrams of SST anomalies computed with the Gmodel-Gill model for three different values of α: 0.15 (a), 0.22 (b), 0.3 (c). A larger value of α indicates a more equatorially confined zonal wind response. The ocean-atmosphere coupling strength was tuned to just below the critical value μ_c.

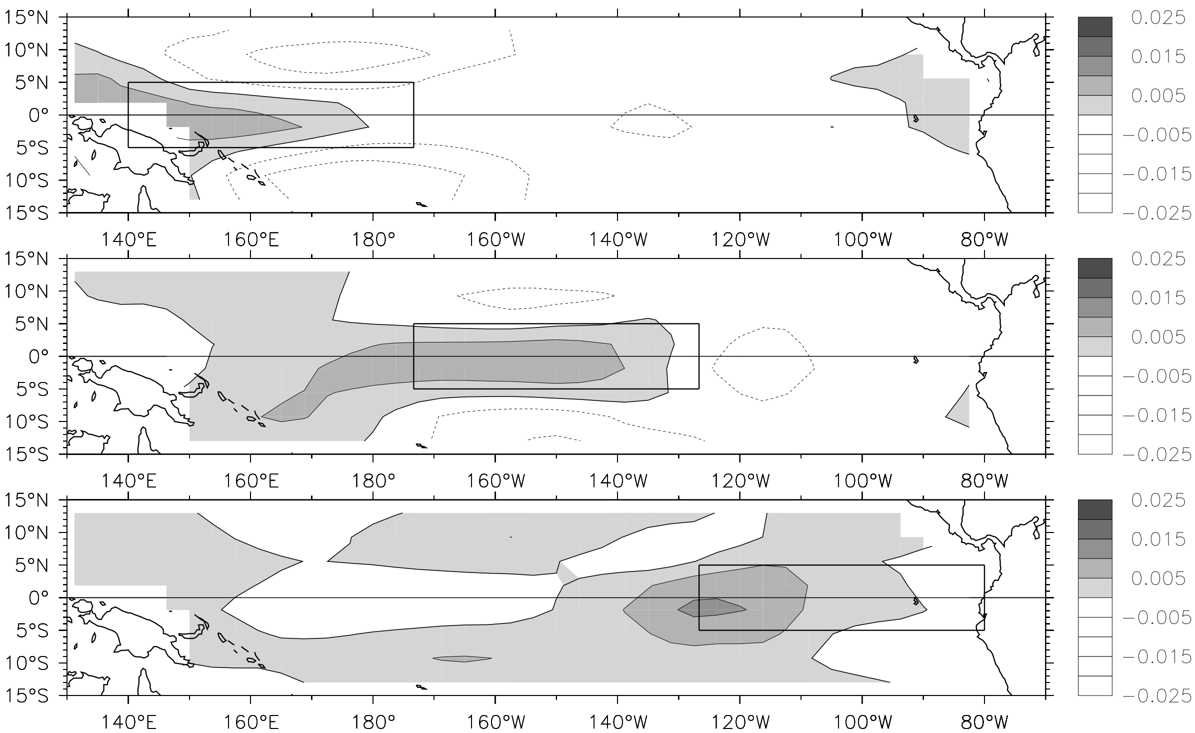

Figure 11: The zonal wind stress response of the CCSM to SST anomalies in boxes from 5°S–5°N and 140°E–173°W, 173°W–127°W, 127°W–80°W respectively. There is no significant difference between the periods 1950–1980 and 2050–2080.

three. The meridional borders of the boxes are at 5°S and 5°N, zonally the boxes are equally divided between 140°E and 80°W.

We switch from $\mathbf{x}$ and $\mathbf{x}'$ to discrete indices k and ℓ, which gives

$$A_{k\ell} = \langle \tau_x' T' \rangle_{km} \langle T' T' \rangle^{-1}_{m\ell} \tag{1}$$

with $A_{k\ell} = A(\mathbf{x}_k, \mathbf{x}'_\ell)$, k an index enumerating τ_x gridpoints, ℓ an index enumerating the T boxes along the equator and $\langle \ldots \rangle$ indicating a time average. The zonal wind response to SST anomalies in the three boxes is shown in Fig. 11. The difference between periods 1950–1980 and 2050–2080 is negligible. The same wind response patterns as determined from the ERA-40 dataset are presented in Fig. 12. Compared to observations, the zonal and meridional extent of the wind response in the CCSM is almost a factor two smaller. When we use the meridional extent of the CCSM wind response pattern in the Gmodel (Fig. 13) we find an ENSO period of approximately 2.5 years, comparable to the ENSO period found in the CCSM.

In the CCSM, the wind response to SST anomalies on the edge of the warm pool is not stronger than the response in the middle of the cold tongue; this is contrary to observations and other models. Also, the westerly wind response to an SST anomaly extends too far east

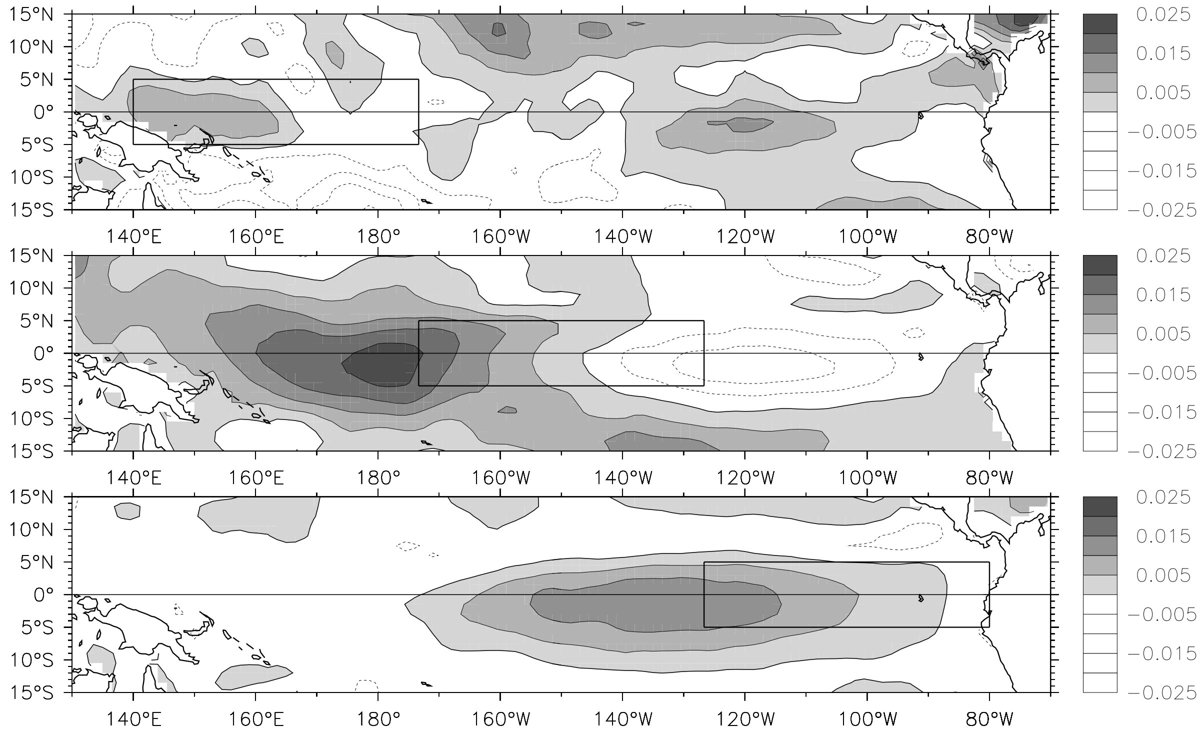

Figure 12: The zonal wind stress response of the ERA-40 reanalysis (observations) to SST anomalies in boxes from 5°S–5°N and 140°E–173°W, 173°W–127°W, 127°W–80°W respectively.

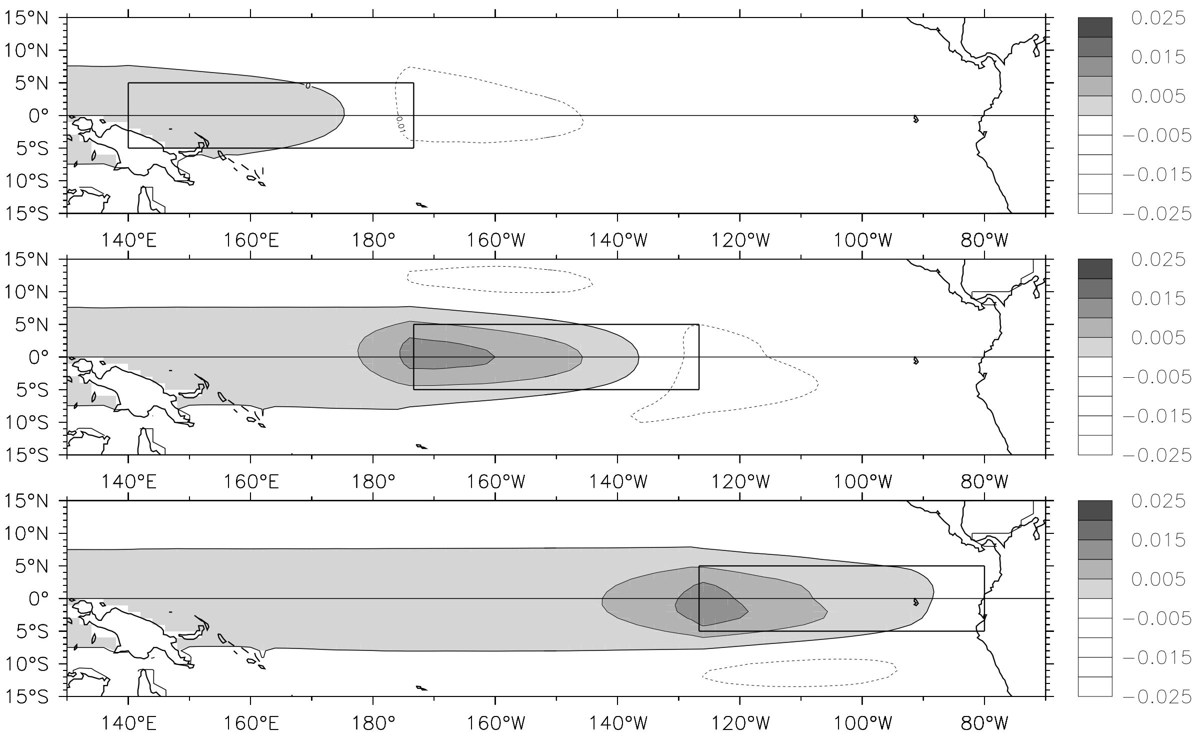

Figure 13: The zonal wind stress response of the linear Gmodel to SST anomalies in boxes from 5°S–5°N and 140°E–173°W, 173°W–127°W, 127°W–80°W respectively. The meridional scale of the wind response was adjusted to match the response of the CCSM in figure 11.

across the SST anomaly. In observations and other models, the zero contour of the zonal wind response is approximately centered above the SST anomaly. The latter two features are linked. Normally, atmospheric heating occurs somewhat west of the SST anomaly due to the climatological zonal SST gradient and the zonal wind response extends east of the heating region (Clarke, 1994). These offsets compensate each other. In the CCSM the dependence on background SST is missing. Therefore atmospheric heating occurs centered above the SST anomaly and the wind response is shifted eastwards compared to observations. The insensitivity of the wind response in the CCSM to background SST is consistent with the fact that there is no change in the wind response due to global warming.

5. Summary and Discussion

Results from a 62 ensemble member simulation with the NCAR-CCSM version 1.4 were used to investigate the changes in ENSO behavior due to the increase of atmospheric greenhouse gases. Under a global climate change of 1.2 K from 2000–2080, the model ENSO variability does not change significantly in each of the ensemble members. The mean equatorial zonal temperature gradient increases slightly but the ENSO period, amplitude and pattern are basically unchanged. The same lack of change was found in this model by Peltier and Solheim (2004) for the much cooler conditions at the Last Glacial Maximum.

One could argue that the warming signal is not strong enough and that larger anomalies are needed to obtain a significant change. Indeed, simulations under $6 \times \mathrm{CO}_2$ conditions have shown a significant change in the ENSO response (Otto-Bliesner and Brady, 2001). On the other hand, in ICMs which represent both the time-mean state and the ENSO delayed oscillator mode quite well, both period and amplitude do change when the radiative equilibrium temperature is increased by only 1 K. One possibility is that these ICMs miss some important physics which influences their response to global warming. Another option is that the coupled feedbacks involved in ENSO are not represented well in the CCSM. We have investigated possible flaws of the CCSM and their effects on the response to global warming.

The insensitivity of ENSO in the CCSM to changes in background temperature suggests that the Pacific climate system is stable. This has been confirmed with an analysis of the attractor dimension of the model which indicates that the model behavior is qualitatively similar to that of a stable system driven by stochastic noise. We have shown that the zonal wind response to SST anomalies in the equatorial Pacific is insensitive to changes in background SST due to the zonal SST gradient, which suggests that the wind response is also insensitive to global warming. The zonal wind response is weaker than in observations and the pattern is too narrow around the equator. These results are robust, due to the large amount of data available from the ensemble for statistical analysis.

Using the linear Gmodel, it was shown that the short ENSO period of the CCSM is related to its narrow zonal wind response pattern around the equator. If the wind response becomes wider, as in the observations, the ENSO period will increase. Also, the narrow wind response pattern results in a more stable system compared to a wider wind response pattern, consistent with the results from Van der Vaart et al. (2000) shown in Fig. 9. A more stable ENSO system is less sensitive to changes in the background state than a system closer to instability.

In conclusion, while the ensemble results may lead one to believe that no significant changes in ENSO are to be expected in the near future, our analysis shows that the insensitivity of ENSO in the CCSM to global warming may be largely due to model errors. This indicates that it is necessary to analyze GCMs with respect to these deficiencies and improve them. Only then can the models be used with some confidence to answer the questions whether and how ENSO will change due to global warming.

Acknowledgements

We thank C. Ammann and B. Otto-Bliesner for their support in porting the CCSM code from NCAR to the TERAS computer system, F. Selten and M. Kliphuis for carefully carrying out the simulations and R. Trompert and colleagues at SARA Computing and Networking Services (Amsterdam) for technical support. The research presented in this paper is supported by the Research Council for Earth and Life Sciences (ALW) of the Netherlands Organization for Scientific Research (NWO). Computer resources were funded by the National Computing Facilities Foundation (NCF) under the project SC-122 with financial support from NWO. Figures were created with Ferret, a product of NOAA's Pacific Marine Environmental Laboratory (www.ferret.noaa.gov).

Appendix: Determination of the dimension of an attractor

The pseudo-state space of dimension M of a generic trajectory of a dynamical system variable $x(t)$ is the space of vectors

$$y(t) = \{x(t),\, x(t-\Delta),\, x(t-2\Delta),\, ...,\, x(t-(M-1)\Delta)\}\ ,$$

where Δ is the so-called delay and M is the embedding dimension. The behavior of the vectors $y(t)$ is related to the dynamics of the underlying dynamical system, as discussed e.g. in the textbook of Nayfeh and Balachandran (1995).

The dimension d of the attractor in pseudo-state phase can be estimated from a long sequence

$$y(t_0),\, y(t_0+\Delta),\, y(t_0+2\Delta),\, ...,\, (t_0+N\Delta) \quad (N >> M)\ ,$$

as follows. First one calculates the cumulative distribution function $C_2(r)$ of distances r between points in the sequence. $C_2(r)$ is obtained from calculating the distances $r(y(t_0+i\Delta), y(t_0+j\Delta))$ for all possible pairs (i,j), and sorting the pairs according to these distances. Instead of a single long sequence, one can also use multiple sequences. This has been done for the ensemble of CCSM simulations. Next one estimates d from the relation

$$C_2(r) \sim r^d$$

that holds for distances r that are sufficiently small that only local properties of the attractor play a role. E.g. if the dimension of the attractor is 2, then around a point on the attractor, on the average 4 times as many attractor points lie within a distance $2r$ as within a distance r. For finite sequences, the above relationship will break down for very small distances where the sampling of the attractor is not adequate. By plotting $C_2(r)$ versus r in a double logarithmic plot, d can be estimated conveniently from the slope of the straight section of the curve. The dimension d will generally depend on the embedding dimension M. The amount of data $x(t)$ limits the maximum value of M for which one can make estimates of d. If the dimension of the attractor of the underlying dynamical system is d_s, one has $d = d_s$ for M above some threshold. A sufficient condition for $d = d_s$ is that $M \geq 2d_s + 1$.

The determination of $C(r)$ is sensitive to contamination of the data by noise, especially at smaller distances (Fraedrich and Wang, 1993). We checked this by adding noise with an amplitude of 0.5 K to the 3-month averages of the ZC-model ouput. Although this causes major changes for $\log(C(r))$ in the range -15 to -10, the picture remains essentially the same for the range $\log(C(r)) \geq -7$ that is shown in Fig. 8.

References

Ammann, C. M., J. T. Kiehl, C. S. Zender, B. L. Otto-Bliesner, and R. S. Bradley, 2005: Coupled simulation of the 20th-century including external forcing. *J. Climate*, in revision.

Boville, B. A., J. T. Kiehl, P. J. Rasch, and F. O. Bryan, 2001: Improvements to the NCAR CSM-1 for transient climate simulations. *J. Climate*, **14**, 164–179.

Burgers, G., M. A. Balmaseda, F. C. Vossepoel, G. J. van Oldenborgh, and P. J. van Leeuwen, 2002: Balanced ocean-data assimilation near the equator. *J. Phys. Oceanogr.*, **32**, 2509–2519.

Cane, M. A., M. M. Münnich, and S. E. Zebiak, 1990: Study of self-excited oscillations of the tropical ocean-atmosphere system. Part I: Linear analysis. *J. Atmos. Sci.*, **47**, 1562–1577.

Clarke, A. J., 1994: Why are surface equatorial ENSO winds anomalously westerly under anomalous large-scale convection? *J. Climate*, **7**, 1623–1627.

Collins, M., 2000: Understanding uncertainties in the response of ENSO to greenhouse warming. *Geophys. Res. Letters*, **27**, 3509–3512.

Collins, M. and coauthors, 2005: El Niño- or La Niña-like climate change? *Clim. Dyn.*, **24**, 89–104, doi:10.1007/s00382-004-0478-x.

Dai, A., T. M. L. Wigley, B. A. Boville, J. T. Kiehl, and L. E. Buja, 2001: Climates of the twentieth and twenty-first centuries simulated by the NCAR climate system model. *J. Climate*, **14**, 485–519.

Dijkstra, H. A. and G. Burgers, 2002: Fluid mechanics of el nino variability. *Annual Review of Fluid Mechanics*, **34**, 531–558.

Fedorov, A. and S. Philander, 2000: Is El Niño Changing? *Science*, **288**, 1997–2002.

Fraedrich, K. and R. Wang, 1993: Estimating the correlation dimension of an attractor from noisy and small datasets based on re-embedding. *Physica*, **D65**, 373–398.

Gill, A. E., 1980: Some simple solutions for heat induced tropical circulation. *Quart. J. Roy. Meteor. Soc.*, **106**, 447–462.

Guilyardi, E., S. Gualdi, J. Slingo, A. Navarra, P. Delecluse, J. Cole, G. Madec, M. Roberts, M. Latif, and L. Terray, 2004: Representing El Niño in coupled ocean-atmosphere GCMs: The dominant role of the atmsphere component. *J. Climate*, **17**, 4623–4629.

Huber, M. and R. Caballero, 2003: Eocene El Nino: Evidence for robust Tropical dynamics in the “Hothouse”. *Science*, **299**, 877–881.

IPCC, 2001: *Climate Change 2001: The Scientific Basis. Contribution of Working Group I to the Third Assessment Report of the Intergovernmental Panel on Climate Change (IPCC) [Houghton, J.T., Y. Ding, D.J. Griggs, M. Noguer, P.J. van der Linden, X. Dai, K. Maskell and C.A. Johnson (eds)]*. Cambridge University Press, Cambridge, UK and New York, NY, 881 pp., also available from www.ipcc.ch.

Jiang, N., J. D. Neelin, and M. Ghil, 1995: Quasi-quadrennial and quasi-biennial varibility in the equatorial Pacific. . *Clim. Dyn.*, **12**, 101–112.

Jones, P. D., T. J. Osborn, K. R. Briffa, C. K. Folland, E. B. Horton, L. V. Alexander, D. E. Parker, and N. A. Rayner, 2001: Adjusting for sampling density in grid box land and ocean surface temperature time series. *J. Geophys. Res.*, **106**, 3371–3380, data are available from http://www.cru.uea.ac.uk/cru/data/temperature.

Kirtman, B. P., 1997: Oceanic Rossby wave dynamics and the ENSO period in a coupled model. *J. Climate*, **10**, 1690–1704.

Knutson, T. R., S. Manabe, and D. Gu, 1997: Simulated ENSO in a global coupled ocean-atmosphere model: Multidecadal amplitude modulation and CO2 sensitivity. *J. Climate*, **10**, 131–161.

Latif, M., K. Sperber, J. Arblaster, P. Braconnot, D. Chen, A. Colman, U. Cubasch, C. Cooper, P. Delecluse, D. De Witt, L. Fairhead, G. Flato, T. Hogan, M. Ji, M. Kimoto, A. Kitoh, T. Knutson, H. Le Treut, T. Li, S. Manabe, O. Marti, C. Mechoso, G. Meehl, S. Power, E. Roeckner, J. Sirven, L. Terray, A. Vintzileos, R. Voß, B. Wang, W. Washington, I. Yoshikawa, J. Yu, and S. Zebiak, 2001: ENSIP: The El Niño Simulation Intercomparison Project. *Clim. Dyn.*, **18**, 255–276.

McPhaden, M. J., A. J. Busalacchi, R. Cheney, J. R. Donguy, K. S. Gage, D. Halpern, M. Ji, P. Julian, G. Meyers, G. T. Mitchum, P. P. Niiler, J. Picaut, R. W. Reynolds, N. Smith, and K. Takeuchi, 1998: The Tropical Ocean Global Atmosphere (TOGA) observing system: A decade of progress. *J. Geophys. Res.*, **103**, 14169–14240, appendix B1.

Nayfeh, A. H. and B. Balachandran, 1995: *Applied Nonlinear Dynamics*. John Wiley, New York, U.S.A.

Neelin, J. D., D. S. Battisti, A. C. Hirst, F.-F. Jin, Y. Wakata, T. Yamagata, and S. E. Zebiak, 1998: ENSO Theory. *J. Geophys. Res.*, **103**, 14,261–14,290.

Noda, A., K. Yoshimatsu, S. Yukimoto, K. Yamaguchi, and S. Yamaki: 1999, Relationship between natural variability and CO_2-induced warming pattern: MRI AOGCM Experiment. *Proc. 10th Symposium on Global Change Studies, Dallas Texas*, American Meteorological Society, Boston, USA, volume 24, 359–362.

Otto-Bliesner, B. and E. Brady, 2001: Tropical Pacific variability in the NCAR Climate System Model. *J. Climate*, **14**, 3587–3607.

Otto-Bliesner, B. L., E. C. Brady, A.-I. Shin, Z. Liu, and C. Shields, 2003: Modeling El Niõ and its tropical teleconnections during the last glacial-interglacial cycle. *Geophys. Res. Letters*, **30**, 2198.

Peltier, W. R. and L. P. Solheim, 2004: The climate of the Earth at Last Glacial Maximum: statistical equilibrium state and a mode of internal variability. *Quat. Sci. Rev.*, **23**, 335–357.

Philander, G. S. and A. Fedorov, 2003: Is El Niño sporadic or cyclic? *Annu. Rev. Earth Planet. Sci. Lett.*, **31**, 579–594.

Philander, S. G., 1990: *El Niño, La Niña and the Southern Oscillation*. Academic Press, San Diego, 293 pp.

Rodbell, D., G. Seltzer, D. M. Anderson, M. B. Abbott, D. B. Enfield, and J. H. Newman, 1999: A 15,000 year record of ENSO-driven alluviation in Southwestern Ecuador. *Science*, **283**, 516–520.

Stricherz, J., D. Legler, and J. O'Brien, 1997: *TOGA Pseudo-stress Atlas 1985–1994, Vol. II: Pacific Ocean*. Florida State University, Tallahassee, FL, USA, 158 pp.

Timmermann, A., F.-F. Jin, and M. Collins, 2004: Intensification of the annual cycle in the tropical Pacific due to greenhouse warming. *Geophys. Res. Letters*, **31**, doi:10.1029/2004GL019442.

Timmermann, A., J. Oberhuber, A. Bacher, M. Esch, M. Latif, and E. Roeckner, 1999: Increased El Nino frequency in a climate model forced by future greenhouse warming. *Nature*, **398**, 694–697.

Trenberth, K. E., , and T. J. Hoar, 1997: The 1990-1995 El Niño-Southern Oscillation event: Longest on record. *Geophys. Res. Letters*, **23**, 57–60.

Tudhope, A. W., C. P. Chilcott, M. T. McCulloch, E. R. Cook, J. Chappell, R. M. Ellam, D. W. Lea, J. M. Lough, and G. Shimmield, 2001: Variability in ENSO through a glacial-interglacial cycle. *Science*, **291**, 1511–1517.

Tziperman, E., L. Stone, M. A. Cane, and H. Jarosh, 1994: El Niño chaos: overlapping of resonances between the seasonal cycle and the Pacific ocean-atmosphere oscillator. *Science*, **264**, 72–74.

Uppala, S. M. and coauthors, 2005: The ERA-40 re-analysis. *Quart. J. Roy. Meteor. Soc.*, submitted.

Van der Vaart, P. C. F., H. A. Dijkstra, and F.-F. Jin, 2000: The Pacific Cold Tongue and the ENSO mode: Unified theory within the Zebiak-Cane model. *J. Atmos. Sci.*, **57**, 967–988.

Von Storch, H. and F. W. Zwiers, 1999,2001: *Statistical Analysis in Climate Research*. Cambridge University Press, The Edinburgh Building, Cambridge CB2 2RU, UK, 484 pp., ISBN 0 521 45071 3 / 0 521 01230 9.

Woodroffe, C. D., M. Beech, and M. K. Gagan, 2003: Mid-late Holocene El Nino variability in the equatorial Pacific from coral microatolls. *Geophys. Res. Letters*, **30**, doi:10.1029/2002GL015868.

Zebiak, S. E. and M. A. Cane, 1987: A model El Niño-Southern Oscillation. *Monthly Weather Review*, **115**, 2262–2278.